

Article

Template-Free Fabrication of Bi_2WO_6 Hierarchical Hollow Microspheres with Visible-Light-Driven Photocatalytic Activity

Yuxue Zhou *, Xiangdong Meng, Ling Tong, Xianghua Zeng and Xiaobing Chen

School of Physical Science & Technology, Yangzhou University, Yangzhou 225002, Jiangsu, China; mengxd@yzu.edu.cn (X.M.); 15861368086@126.com (L.T.); xhzeng@yzu.edu.cn (X.Z.); xbchen@yzu.edu.cn (X.C.)

* Correspondence: yxzhou@yzu.edu.cn; Tel.: +86-514-8797-5466

Academic Editor: José Pérez

Received: 24 June 2016; Accepted: 13 September 2016; Published: 22 September 2016

Abstract: Highly hierarchical hollow bismuth tungstate (Bi_2WO_6) microspheres self-assembled by thin nanoplates have been fabricated via a facile template-free solvothermal route. The possible growth pattern and formation mechanism of hierarchical hollow Bi_2WO_6 microspheres was investigated. The excellent visible-light-driven photocatalytic performance on rhodamine B (RhB) degradation was displayed by hierarchical hollow Bi_2WO_6 microspheres. Such well-organized hierarchical hollow Bi_2WO_6 microspheres show potential application in water treatment fields by full use of solar energy.

Keywords: bismuth tungstate (Bi_2WO_6); semiconductor photocatalyst; visible-light-driven; water treatment

1. Introduction

In recent decades, a great deal of attention has been given to visible-light responding semiconductor photocatalysts in the degradation of organic pollutants in water for solving environmental pollution problems by the efficient full utilization of solar energy [1,2]. Bismuth tungstate (Bi_2WO_6), a semiconductor photocatalyst with a narrow width of band gap and as one of the simplest members of the Aurivillius oxide group constructed by alternating $(\text{Bi}_2\text{O}_2)^{2+}$ layers and perovskite-like $(\text{WO}_4)^{2-}$ layers, was discovered to possess promising visible-light-driven photocatalytic activity on water treatment [3,4], and it also contains ferroelectric piezoelectricity and nonlinear dielectric susceptibility [5], all of which are fascinating to materials scientists. Bi_2WO_6 photocatalysts in micro- and nano-scale with various morphologies (such as nanoparticles [6], square nanoplates [7], and flower-like microstructures [8,9]) have been explored in order to enhance their visible-light responding photocatalytic performance in view of close correlations between the photocatalytic activity and the morphology and the microstructure of semiconductor photocatalysts.

Particularly, the hierarchical hollow architectures of Bi_2WO_6 exhibit superior visible-light-driven photocatalytic activity due to well-defined interior voids, larger surface area, and more efficient use of the light source via multiple reflections of light within the interior cavity [10,11]. Till now, Bi_2WO_6 hollow architectures have been precipitated in some diverse ways. For instance, Dai et al. [12] synthesized Bi_2WO_6 hollow microspheres in presence of polyvinyl pyrrolidone (PVP) surfactant as “soft template” in reaction solution, Li et al. [13] got Bi_2WO_6 hollow microspheres using polystyrene (PS) particles as a “hard template” via a hydrothermal process, and Shang et al. [14] obtained Bi_2WO_6 hollow nanocages in use of colloidal carbon as a “hard template” in a solvothermal way. However, the procedures from usage of templates are somehow complicated and of high cost including template modification, precursor attachment, and core removal, which limits large-scale applications of Bi_2WO_6 hollow architectures in water treatment. Therefore, template-free fabrication of hierarchical Bi_2WO_6 hollow spheres is highly appreciated by which the preparation procedure can obviously be

simplified and become cost-effective, it will make important progress for enhancing the photocatalytic performance of Bi_2WO_6 hollow microspheres and for their potential larger scale application on degradation of organic pollutants in water treatment.

Herein, we obtain Bi_2WO_6 hierarchical hollow microspheres assembled by thin nanoplates in one pot template-free solvothermal way. A possible formation mechanism of Bi_2WO_6 hierarchical hollow microspheres was explored. The precipitated Bi_2WO_6 hierarchical hollow microspheres display excellent visible-light-driven photocatalytic activity on degradation of rhodamine B (RhB) aqueous solution. Such an obtained hollow Bi_2WO_6 catalyst displays possible utilization in water treatment through full use of solar energy.

2. Experimental

2.1. Synthesis

The chemical reagents $\text{Bi}(\text{NO}_3)_3 \cdot 5\text{H}_2\text{O}$, $\text{Na}_2\text{WO}_4 \cdot 2\text{H}_2\text{O}$, ethylene glycol (EG), and ethanol (EA) in this work were of analytical reagent bought from Sinopharm Chemical Reagent Company (Shanghai, China) without purification more. In a typical procedure on fabrication of Bi_2WO_6 hierarchical hollow spheres, 2 mmol $\text{Bi}(\text{NO}_3)_3 \cdot 5\text{H}_2\text{O}$ and 1 mmol $\text{Na}_2\text{WO}_4 \cdot 2\text{H}_2\text{O}$ were firstly dissolved in 15 mL EG and EA mixture solution ($V_{\text{EG}}:V_{\text{EA}} = 1:2$), respectively. Then the above two solutions were mixed and stirred for 30 min to obtain a precursor suspension at room temperature. In the end, a 50 mL Teflon-line autoclave was used to hold the resulting mixture and heated at 160 °C for 12 h. After the autoclave was cooled naturally, the precipitate was obtained by centrifugation with distilled water and absolute ethanol washing for several times to get rid of the impurity, then dried at 80 °C in a drying oven for 6 h. Commercial nano TiO_2 with size of 5–10 nm and 4-chlorophenol (4-CP) were bought from Shanghai Aladdin Bio-Chem Technology Company (Shanghai, China).

2.2. Characterization

The obtained Bi_2WO_6 products were characterized by X-ray diffraction (XRD, Philips X' Pert Pro Super, Philips, Amsterdam, The Netherlands), field emission scanning electron microscopy (FESEM, Japan Hitachi S-4800, Hitachi, Tokyo, Japan), transmission electron microscope (TEM, Holland Philips Tecnai-12, Philips, Amsterdam, The Netherlands), high-resolution transmission electron microscopy (HRTEM, FEI Tecnai G2 F30 S-TWIN, FEI, Hillsboro, OR, USA), X-ray photoelectron spectrometer (XPS, ESCALab 250Xi, Thermo Scientific, Waltham, MA, USA). Ultra violet-visible diffuse reflectance spectra (DRS) were recorded on a ultraviolet (UV)-vis diffuse reflectance spectrum (Varian Cary 5000, Varian, Palo Alto, CA, USA). Brunauer–Emmett–Teller (BET) surface area was got by using a Micrometrics ASAP 2020 analyzer (Micrometrics, Norcross, GA, USA).

2.3. Photocatalytic Activity Test

Photocatalytic activities of the Bi_2WO_6 hierarchical hollow spheres samples were evaluated by the degradation of RhB and 4-CP under visible-light irradiation using a 300 W Xe lamp with a 420 nm cut-off filter as a light source and degradation of aqueous of aqueous RhB solution from Bi_2WO_6 hierarchical hollow spheres were also carried out under UV light from 250 W UV lamp ($\lambda = 254$ nm). In each experiment, 100 mg photocatalysts were added into 100 mL RhB of solution (1×10^{-5} mol/L) or 4-CP of solution (10 mg/L). The suspension was firstly magnetically stirred for 30 min without light to reach the adsorption-desorption equilibrium from the photocatalysts and RhB (4-CP). Then the solution was under UV or visible-light irradiation with magnetically stirring. During illumination, around 4 mL of suspension was got out from the reactor at a timed interval and centrifuged to get rid of the bottom photocatalysts. Then, the filtrates were examined by marking changes of the absorption band maximum (553 nm from RhB and 224 nm from 4-CP) in the UV-vis spectra by using a Shimadzu

UV-2500 PC spectrophotometer (Shimadzu, Suzhou, China). The following equation was used to calculate the photocatalytic efficiency:

$$\text{Removal efficiency (\%)} = \frac{C_0 - C}{C_0} \times 100\% \quad (1)$$

where C_0 and C represent the initial concentration of RhB (4-CP) in aqueous solution before illumination and the concentration of RhB (4-CP) after timed irradiation, separately.

3. Results and Discussion

3.1. Structure and Morphology

Hierarchical hollow Bi_2WO_6 microspheres assembled by thin nanoplates have been directly fabricated in a template-free solvothermal way under 160°C for 12 h. The XRD pattern of the product is shown in Figure 1d, that eight major sharp reflection peaks locating at $2\theta = 28.15^\circ, 33.15^\circ, 47.34^\circ, 55.89^\circ, 58.39^\circ, 68.61^\circ, 75.71^\circ,$ and 78.01° can be indexed to the well crystalline, orthorhombic phase of Bi_2WO_6 with standard values (lattice parameters of $a = 5.457 \text{ \AA}, b = 5.436 \text{ \AA},$ and $c = 16.427 \text{ \AA},$ JCPDS No. 73-1126). And not any other phases or impurities were detected in this pattern. Figure 1a shows the panoramic FESEM image of a typical sample containing plenty of Bi_2WO_6 hierarchical hollow microspheres with diameters of ca. $1.5\text{--}2.0 \mu\text{m}$. The higher magnification image in Figure 1b clearly reveals that some Bi_2WO_6 hollow microspheres are highly hierarchical with numerous thin nanoplates orderly aggregated on their outer surface. Figure 1c is the enlarged image of an individual Bi_2WO_6 hierarchical hollow sphere, further clearly illustrating its hollow structure with large open void and thin nanoplates with an average thickness of ca. 25 nm assembling on Bi_2WO_6 outer surface to construct the hierarchical hollow pattern of Bi_2WO_6 microspheres.

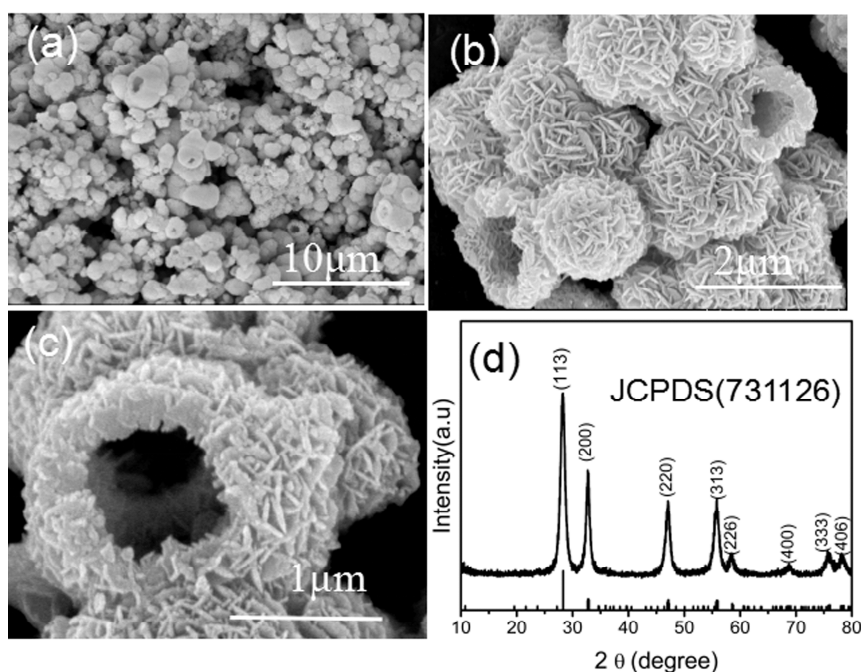


Figure 1. (a) A general view; (b,c) higher magnification field emission scanning electron microscopy (FESEM) images; and (d) X-ray diffraction (XRD) pattern of the hierarchical bismuth tungstate (Bi_2WO_6) hollow spheres prepared at 160°C for 12 h.

In addition, the morphological information of the as-prepared Bi_2WO_6 hierarchical hollow spheres was investigated further by TEM images. Figure 2a is the bright-field TEM image of several Bi_2WO_6

hollow microspheres, which indicates that the hierarchical hollow micro-structures assembled orderly from a large quantity of thin nanoplates on the outer surface, in accord with the characterization of FESEM images in Figure 1 from the Bi_2WO_6 hollow sample. Figure 2b is the higher magnification TEM image recorded at certain edge of individual hollow architecture, further exhibiting that it is actually built from two dimensional thin nanosheets. Figure 2c is the enlarged lattice-resolved HRTEM image taken from the white rectangle marked part in Figure 2b, clear lattice fringes can be seen and it showed that the spacing of the observed lattice plane is approximately 0.315 nm, which is consistent with the spacings from the (113) plane of orthorhombic Bi_2WO_6 phase.

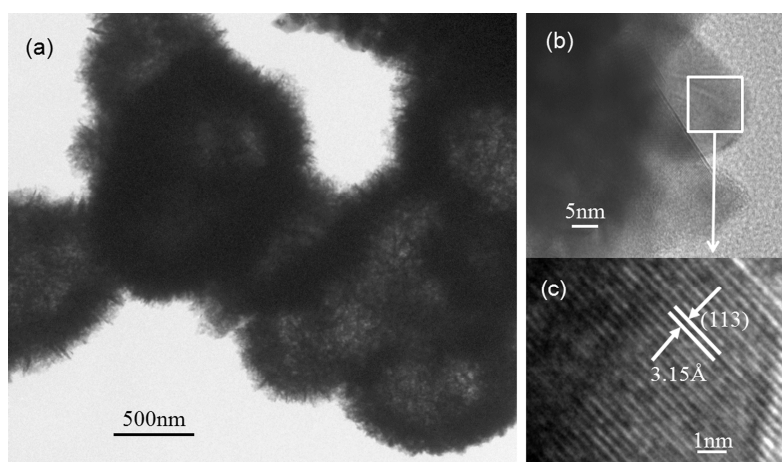


Figure 2. (a) General and (b) higher magnification transmission electron microscope (TEM) image of hierarchical Bi_2WO_6 hollow spheres; and (c) enlarged high-resolution transmission electron microscopy (HRTEM) image taken on a white rectangle marked part in Figure 2b. The hierarchical Bi_2WO_6 hollow spheres were synthesized at 160 °C for 12 h.

Figure 3 is the X-ray photoelectron spectroscopy (XPS) analysis of as obtained hierarchical Bi_2WO_6 hollow microspheres which is performed in order to investigate the chemical states and surface composition of the elements in Bi_2WO_6 hollow microspheres. The XPS full survey spectra displayed Bi, W, and O elements from Bi_2WO_6 hollow microspheres, and C element is from the binder (Figure 3a), the high-resolution spectra of single Bi, W, and O element were displayed separately in Figure 3b–d. The binding energies of 159.2 eV and 164.5 eV (Figure 3b) are attributed to the corresponding $4f_{7/2}$ and $4f_{5/2}$ of Bi^{3+} element. Two peaks centered at 35.7 eV and 37.8 eV (Figure 3c) are respectively assigned to $4f_{7/2}$ and $4f_{5/2}$ from W^{6+} element which is in accord with the reported values [15]. The sharp and a slightly non-symmetric O_{1s} peak located at the binding energy of 529.9 eV (Figure 3d) may be from the main contribution of crystal lattice oxygen and adsorbed oxygen in the oxide [16].

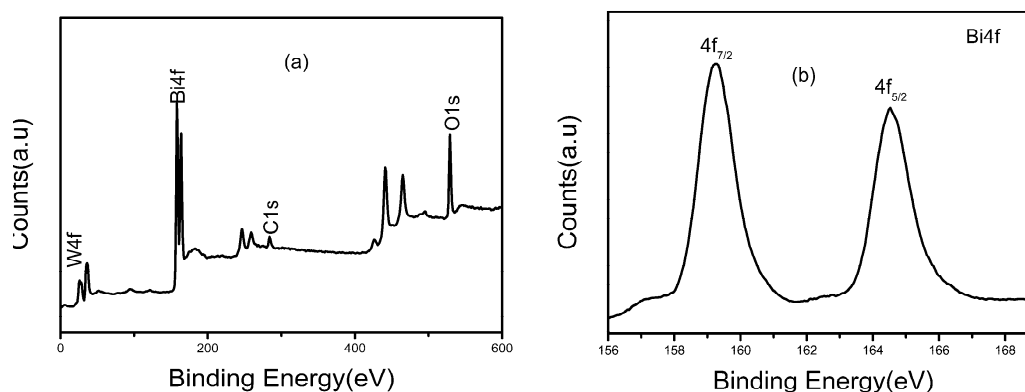


Figure 3. Cont.

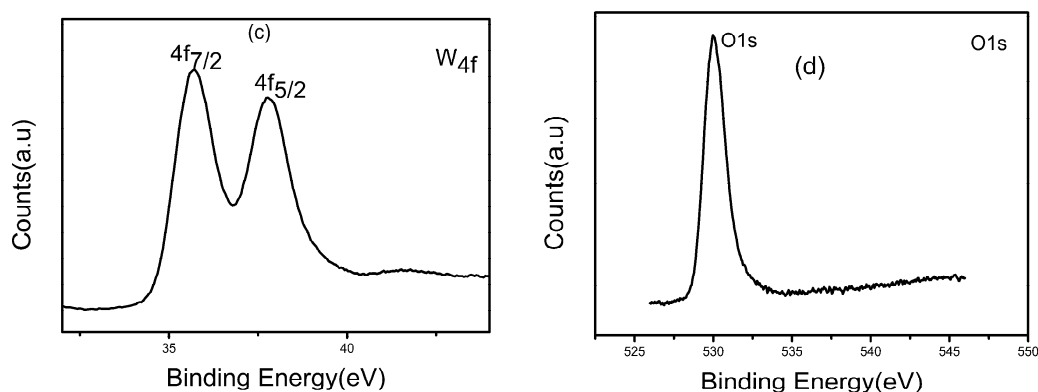


Figure 3. X-ray photoelectron spectroscopy (XPS) spectra of the hierarchical Bi_2WO_6 hollow microspheres: (a) the typical survey; the high-resolution spectra of (b) Bi_{4f} , (c) W_{4f} , and (d) O_{1s} .

3.2. Ultraviolet-Visible Diffuse Reflectance Spectra Analysis

The optical absorption property of the as obtained Bi_2WO_6 hierarchical hollow microsphere was conducted by the UV-visible DRS (Figure 4), from which we can see that the Bi_2WO_6 hierarchical hollow microspheres exhibited strong photo-absorption in visible-light region and have a steep absorption edge of 443 nm, the spectra indicates that the visible-light absorption was caused by intrinsic band-gap transition instead of the transition from the impurity level [17]. As to a crystalline semiconductor, the optical absorption near the band edge corresponds to the equation $\alpha h\nu = A(h\nu - E_g)^n$ for a direct band gap semiconductor material, where α , h , ν , E_g , and A are separately the absorption coefficient, Plank constant, light frequency, band gap, and a constant. Among which n decides the characteristics of the transition in a semiconductor and the n value of Bi_2WO_6 hollow microsphere equals to 2 [12]. The optical band gap (E_g) was obtained by extrapolation of the plot (the inset of Figure 4) of $(\alpha h\nu)^{1/2}$ versus $h\nu$ and was calculated to be 2.76 eV, that was close to that of the previously reported Bi_2WO_6 microstructures (2.75 eV) [18]. The color of the obtained Bi_2WO_6 hierarchical hollow microsphere was faint-yellow, as can be expected from the absorption spectrum. According to the above UV-vis DRS analysis results, we may conclude that the as-obtained Bi_2WO_6 hierarchical hollow microspheres can be suitable for photocatalytic degradation of organic pollutants in aqueous solution under visible-light irradiation in water treatment.

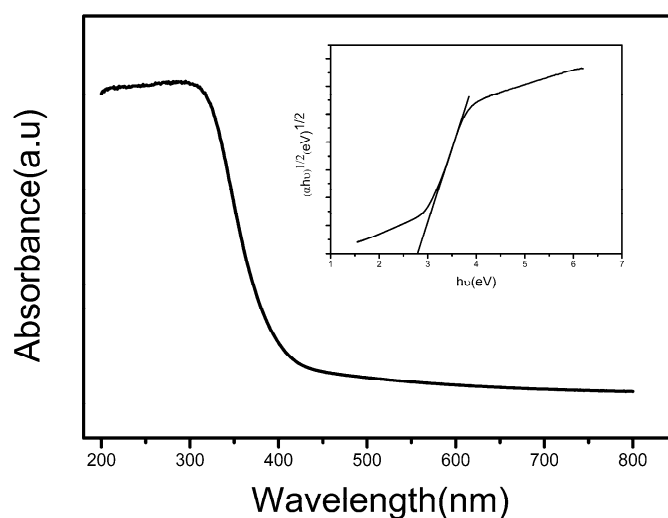


Figure 4. Ultraviolet (UV)-vis diffuse reflectance spectra of hierarchical Bi_2WO_6 hollow microspheres. The insert is the corresponding $(\alpha h\nu)^{1/2}$ versus photon energy plots. The sample was fabricated at 160°C for 12 h.

3.3. Brunauer–Emmett–Teller Surface Area Analysis

The N_2 adsorption and desorption isotherms and the corresponding curves of the pore size distribution (PSD) shown in Figure 5 were executed to get the BET specific surface area and PSD of the obtained Bi_2WO_6 hierarchical hollow microspheres. The BET surface area of Bi_2WO_6 hollow microspheres was calculated to be $36.83 \text{ m}^2/\text{g}$ from the N_2 adsorption and desorption isotherms, which is higher than that of typical SSR- Bi_2WO_6 ($0.6 \text{ m}^2/\text{g}$) [19], Bi_2WO_6 nanocages ($14.6 \text{ m}^2/\text{g}$) [13] and Bi_2WO_6 hollow tubes ($32.0 \text{ m}^2/\text{g}$) [20]. PSD curve inserted in Figure 5 indicates there are two sizes of mesopores existing in Bi_2WO_6 hierarchical hollow microspheres, one is about 2.3 nm, the other is about 22.5 nm. The smaller mesopores may be caused by the porosity within Bi_2WO_6 nanoplates, while the larger ones can be attributable to pores formed between self-assembled Bi_2WO_6 nanoplates [21]. Considering the larger BET surface area and unique hierarchical hollow structure of Bi_2WO_6 microspheres may be effective for efficient visible-light harvesting and introducing reactants into the interior hollow space [21,22], the visible-light-driven photocatalytic activity of Bi_2WO_6 hierarchical hollow microspheres could be enhanced.

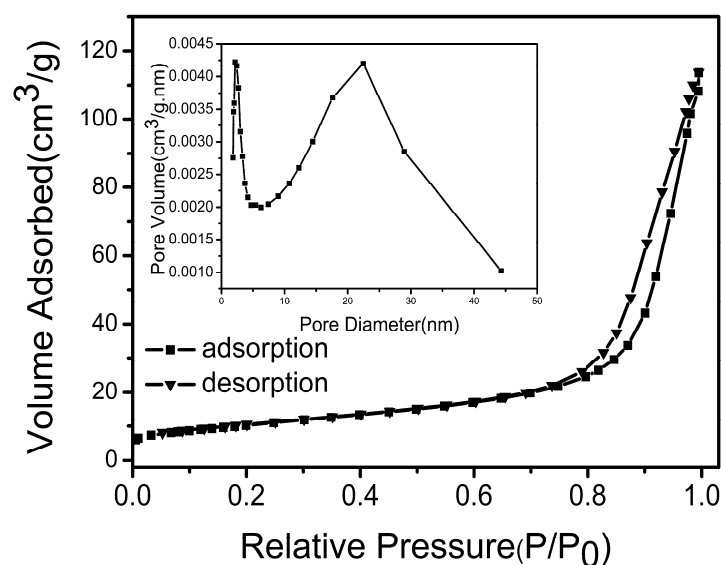


Figure 5. N_2 adsorption and desorption isotherms and pore size distribution (PSD) curve (insert) for hierarchical Bi_2WO_6 hollow microspheres.

3.4. Formation Mechanism

In order to better understand the formation mechanism of the Bi_2WO_6 hierarchical hollow microspheres, the time-dependent experiments were performed and the products formed at various solvothermal reaction times were characterized by XRD patterns (Figure S1 in Supplementary Materials) and FESEM images (Figure 6). Initially, the obtained sample was mainly composed of numerous microspheres with smooth surface and several small nanoparticles after reaction for 1 h, as shown in Figure 6a. When the reaction proceeded to 2 h, microspheres with rough surfaces were formed (Figure 6b). Then hollow microsphere with larger void and nanosheets assembling on the outer surface was obtained while the cores in the center of microsphere disappeared as the reaction time extended to 4 h (Figure 6c). The XRD patterns showed that the phase of the products changed from amorphous to pure and crystallized Bi_2WO_6 orthorhombic phase after the 4 h reaction (Figure S1).

Further comparative experiments were carried out by adjusting the volume ratio of the solvent EG and solvent EA while keeping other experimental parameters unchanged, which indicates that the final architecture and morphology of the products can be varied by adding different EG and EA content. When the volume ratio of EG and EA ($V_{EG}:V_{EA}$) was decreased to 1:5, Bi_2WO_6 flower-like microspheres occurred (Figure S2a), irregular plate-like aggregates come into being while the solvent

was pure EG without EA ($V_{EG}:V_{EA} = 0:1$, Figure S2b), it indicates that suitable EG and EA content in reaction solution was in favor of the formation of hollow Bi_2WO_6 microspheres. The XRD patterns showed that the obtained precipitates were pure Bi_2WO_6 phase (Figure S3).

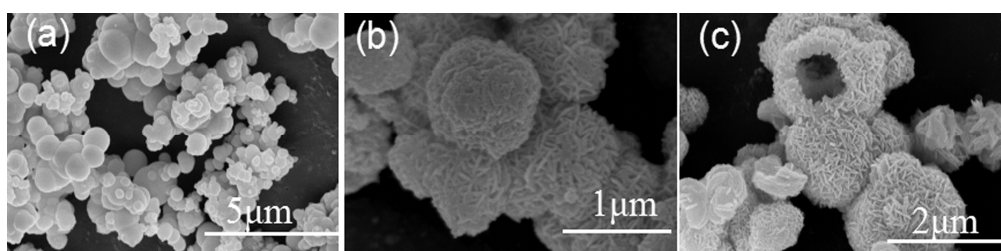
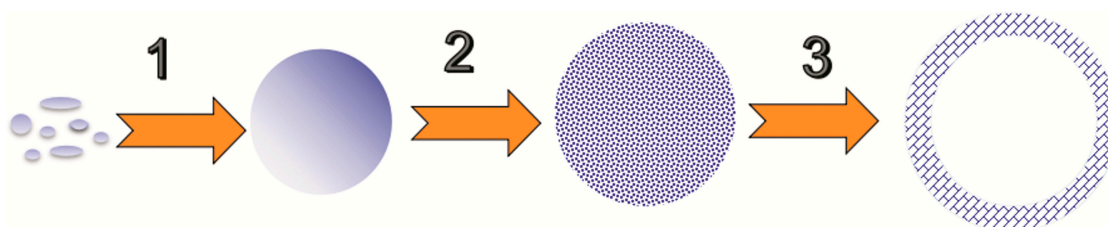


Figure 6. Scanning electron microscopy (SEM) images of samples obtained at 160 °C for (a) 1 h, (b) 2 h, and (c) 4 h, respectively.

Based on the above comparative experimental results, we speculated that the possible growth pattern and formation mechanism of such hierarchical hollow Bi_2WO_6 microspheres assembled by thin nanoplates could be attributed to the typical Ostwald ripening mechanism, which has been employed as a template-free strategy to get inorganic hollow structures via an “inside-out” mechanism that thermo-dynamically less stable matter in the core of solid aggregates is dissolved and scattered into the surface, the hollow structures were obtained by continuous evacuation of the core materials [23,24]. Many hollow nano/micro structures have been reported according to this classic Ostwald ripening formation mechanism, such as hierarchical flower-like Bi_2MoO_6 hollow spheres [25], CeO_2 hollow nanospheres [26], nanosheet-assembled ZnFeO_4 hollow microspheres [27], double-wall Cu_2O hollow spheres [28]. Scheme 1 illustrates the possible representation for shaped process of as-obtained hierarchical hollow Bi_2WO_6 microspheres (Steps 1–3). At the initial stage of the solvothermal reaction process, tiny particles were precipitated and had a tendency to aggregate into amorphous solid microspheres caused by decreasing the high surface energy of the nanoparticles (Step 1 in Scheme 1, nucleation and self-aggregation), then microspheres with rough surface were obtained (Step 2 in Scheme 1), with solvothermal reaction time prolonging, the hollowing procedure occurs as the interior parts of the solid microspheres dissolved due to mass diffusion and Ostwald ripening formation mechanism, at the same time the rough outer surface of hollow Bi_2WO_6 microspheres were assembled by thin nanosheets in view of anisotropic growth and layered crystal features of Bi_2WO_6 , finally hierarchical hollow Bi_2WO_6 microspheres aggregated by two dimensional thin nanoplates were formed (Step 3 in Scheme 1).



Scheme 1. Illustration of the formation process of the hierarchical Bi_2WO_6 hollow spheres obtained at 160 °C for 12 h.

3.5. Photocatalytic Activity

Figure 7a shows the investigated visible-light-driven photocatalytic decomposition abilities of RhB (a widely used dye with characteristic absorption band at 553 nm) aqueous solution from the as obtained Bi_2WO_6 samples precipitated under various volume ratio of EG and EA in reaction solution. We can see that our prepared hierarchical hollow Bi_2WO_6 microspheres assembled by thin nanoplates

($V_{EG}:V_{EA} = 1:2$) showed higher visible-light-driven photocatalytic performance than that of Bi_2WO_6 flower-like microspheres ($V_{EG}:V_{EA} = 1:5$), and of irregular plate-like aggregates ($V_{EG}:V_{EA} = 0:1$) on RhB degradation, realizing 95% degradation of RhB under visible-light illumination only within 40 min, and the hierarchical hollow Bi_2WO_6 microspheres also indicate much higher photocatalytic performance than commercial nano TiO_2 (anatase, 5–10 nm) under visible-light irradiation, while the blank test showed the photodegradation efficiency was only 5% within 40 min, demonstrating RhB degradation is extraordinarily slow without Bi_2WO_6 photocatalyst only under visible-light illumination. The empty structure of as prepared hollow spheres may promote both the outer and inner surfaces of the photocatalyst to contact with the objective organic contamination more easily [29], and light harvesting efficiency can be effectively enhanced in view of special microstructures of the hollow sphere [30], thus the visible-light-driven photocatalytic performance of highly hierarchical hollow Bi_2WO_6 microspheres on degradation of RhB contaminants in aqueous solution was raised. However, we investigated the photocatalytic performance of Bi_2WO_6 hollow microspheres under UV-light ($\lambda = 254 \text{ nm}$) and the photodegradation efficiency was 26% within 40 min (see Figure S4), it tells us that Bi_2WO_6 hollow microspheres show much weaker photocatalytic activity under UV-light irradiation. Dai et al. [31] reported weaker photocatalytic performance of visible-light-driven photocatalysts irradiated under light with wavelength of around 450 nm (excluding absorption and self-degradation of organic dyes under visible-light with wavelength of $\lambda > 480 \text{ nm}$) than that of the photocatalysts illuminated under visible-light with wavelength of $\lambda > 420 \text{ nm}$. Therefore, from the above analysis, we may conclude that the photocatalytic activity from Bi_2WO_6 hollow microspheres will display best under visible-light illumination with wavelength of $\lambda > 420 \text{ nm}$.

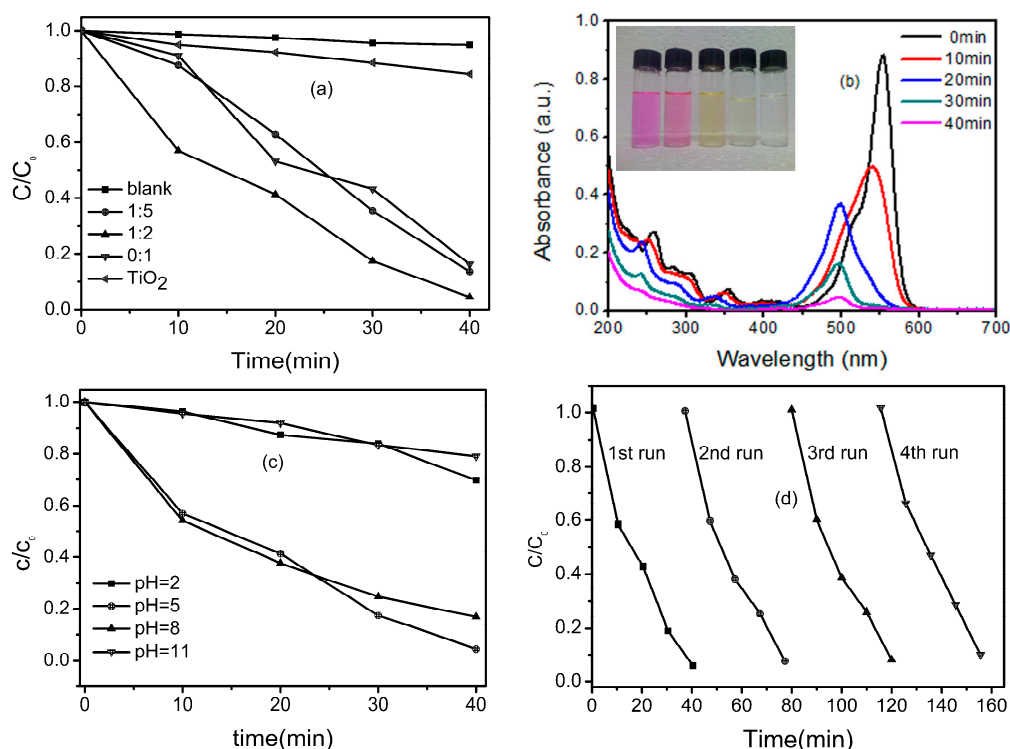


Figure 7. (a) Photocatalytic activities on degradation of RhB from Bi_2WO_6 samples obtained at different volume ratio of ethylene glycol (EG) and ethanol (EA) in reaction solution. (b) The temporal evolution of the absorption spectra of the RhB solution under visible-light irradiation in the presence of 100 mg hierarchical hollow Bi_2WO_6 microspheres, the insert is the corresponding time-dependent color changes of the RhB solution. (c) Photocatalytic performance on degradation of RhB in aqueous solution with various pH values. (d) Cyclability of photocatalytic activity from hierarchical hollow Bi_2WO_6 microspheres under visible-light irradiation.

Figure 7b exhibits the temporal evolution of the absorption spectra of RhB aqueous solution mediated by the hierarchical hollow Bi_2WO_6 microspheres assembled by nanoplates under visible-light irradiation, indicating that the intensity of major absorption peaks from RhB was gradually decreased along with the peak blue shift as the exposure time was extended, which is consistent with the color changes of the aqueous solution from initial pink to a light yellow-green and then to transparent (insert in Figure 7b), indicating that the de-ethylation of RhB is a step-wise way from tetra-ethylated rhodamine structure to tri-, di-, mono-ethylated rhodamine and to rhodamine, and finally the conjugate structure was almost broken and converted into CO_2 and H_2O , in accordance with the previous reports [32].

Figure 7c illustrates the influence of different pH values on the photocatalytic activities of our nanoplate-assembled hollow Bi_2WO_6 microspheres in RhB aqueous solution. From which we can obviously see that Bi_2WO_6 hollow microspheres show the highest photocatalytic activity in neutral solution within 40 min compared with such Bi_2WO_6 photocatalyst samples in strong acidic or alkaline aqueous solution. To make things worse, the degradation rate of RhB only reaches 20% in the basic solution at $\text{pH} = 11$ under exposure to visible light for 40 min. Considering the pH variation has influence on the dye structure, surface charge of the photocatalyst [33], and the constituent of photocatalyst [34], it is well-balanced to see the difference of photocatalytic activities from the same photocatalyst in various pH values solution. Bi_2WO_6 was unstable and completely transformed to H_2WO_4 and Bi_2O_3 in much more acidic solution, that may be the reason for weaker photocatalytic activity of hollow Bi_2WO_6 microspheres [34]. Because the surface charge of Bi_2WO_6 catalyst may be transformed and the adsorption of RhB was decreased due to charge repulsion in strong alkaline solution [33], the RhB degradation reaction was slowed down.

The cycle experiments of RhB degradation by hierarchical hollow Bi_2WO_6 microspheres under visible-light irradiation were further carried out in order to assess the reusability and stability of the Bi_2WO_6 hollow microspheres as photocatalysts for practical application in water treatment. Figure 7d reveals that the photo degradation performance of as-obtained hollow Bi_2WO_6 microspheres has no significant loss after four cycles. Figure S5 shows the XRD and SEM image of hollow Bi_2WO_6 microspheres after RhB photocatalytic degradation reaction. The XRD pattern of hollow Bi_2WO_6 microspheres after RhB degradation indicates no change in position of the diffraction peaks and no other phases except Bi_2WO_6 phase were observed, which tells us that the structure of Bi_2WO_6 phase was not changed. Moreover, the SEM image of the used Bi_2WO_6 photocatalyst did not show any obvious change and displays the reserved hollow microstructures of Bi_2WO_6 photocatalysis. From the above, we can conclude the high stability and durability of our tested hierarchical hollow Bi_2WO_6 microspheres.

The photodegradation of colorless 4-CP as a target molecule was also carried out to further demonstrate the photocatalytic performance under visible-light irradiation. Figure S6 shows that photodegradation efficiency of 4-CP was 44% within 6 h, although the degradation rate was slower than reported nanosized Bi_2WO_6 catalyst (higher than 90% within 6 h) [18], it really more illustrates the visible-light-driven photocatalytic activity of hollow Bi_2WO_6 microspheres.

4. Conclusions

In summary, a simple one-pot solvothermal way was introduced to obtain numerous thin nanoplate aggregated hollow Bi_2WO_6 microspheres with hierarchies without any templates in reaction solution. The Ostwald ripening formation mechanism was speculated on growth pattern of hierarchical hollow Bi_2WO_6 microspheres self-assembled by nanoplates. The well-defined hollow Bi_2WO_6 microspheres exhibit much better photocatalytic activity on degradation of RhB in water under visible light irradiation over other morphological Bi_2WO_6 products in view of their particular hierarchical hollow architectures with big cavities, larger surface area, and permeability. Further, such hierarchical hollow Bi_2WO_6 microspheres with high photocatalytic performance fabricated in

a cost-effective solvothermal method shows potential application in water treatment especially in organic pollutant deterioration under visible-light irradiation.

Supplementary Materials: The following are available online at www.mdpi.com/1996-1073/9/10/764/s1.

Acknowledgments: This work was supported by Natural Science Foundation of China for the Youth (No. 21101135) and National Natural Science Foundation of China (No. 61474096).

Author Contributions: Yuxue Zhou designed the experiments and wrote the paper; Yuxue Zhou and Ling Tong performed the experiments; Yuxue Zhou and Xiangdong Meng analyzed the data; Xianghua Zeng and Xiaobing Chen contributed materials and analysis tools.

Conflicts of Interest: The authors declare no conflict of interest.

References

1. Cheng, X.L.; Jiang, J.S.; Hu, M.; Mao, G.Y.; Liu, Z.W.; Zeng, Y.; Zhang, Q.H. Liquid–liquid interface-assisted solvothermal synthesis of durian-like α - Fe_2O_3 hollow spheres constructed by nano-polyhedrons. *Cryst. Eng. Comm.* **2012**, *14*, 3056–3062. [[CrossRef](#)]
2. Lin, Q.Y.; Li, L.; Liang, S.J.; Liu, M.H.; Bi, J.H.; Wu, L. Efficient synthesis of monolayer carbon nitride 2D nanosheet with tunable concentration and enhanced visible-light photocatalytic activities. *Appl. Catal. B Environ.* **2015**, *163*, 135–142. [[CrossRef](#)]
3. Zhang, N.; Ciriminna, R.; Pagliaro, M.; Xu, Y.J. Nanochemistry-derived Bi_2WO_6 nanostructures: Towards production of sustainable chemicals and fuels induced by visible light. *Chem. Soc. Rev.* **2014**, *43*, 5276–5287. [[CrossRef](#)] [[PubMed](#)]
4. Zhou, Y.G.; Zhang, Y.F.; Lin, M.S.; Long, J.L.; Zhang, Z.Z.; Lin, H.X.; Wu, J.C.-S.; Wang, X.X. Monolayered Bi_2WO_6 nanosheets mimicking heterojunction interface with open surfaces for photocatalysis. *Nat. Commun.* **2015**, *6*, 8340–8347. [[CrossRef](#)] [[PubMed](#)]
5. Feteira, A.; Sinclair, D.C. Microwave dielectric properties of low firing temperature $\text{Bi}_2\text{W}_2\text{O}_9$ Ceramics. *J. Am. Ceram. Soc.* **2008**, *91*, 1338–1341. [[CrossRef](#)]
6. Jiang, L.; Wang, L.Z.; Zhang, J.L. A direct route for the synthesis of nanometer-sized Bi_2WO_6 particles loaded on a spherical MCM-48 mesoporous molecular sieve. *Chem. Commun.* **2010**, *46*, 8067–8069. [[CrossRef](#)] [[PubMed](#)]
7. Shang, M.; Wang, W.Z.; Sun, S.M.; Zhou, L.; Zhang, L. Bi_2WO_6 nanocrystals with high photocatalytic activities under visible light. *J. Phys. Chem. C* **2008**, *112*, 10407–10411. [[CrossRef](#)]
8. Chen, Z.; Qian, L.W.; Zhu, J.; Yuan, Y.P.; Qian, X.F. Controlled synthesis of hierarchical Bi_2WO_6 microspheres with improved visible-light-driven photocatalytic activity. *Cryst. Eng. Comm.* **2010**, *12*, 2100–2106. [[CrossRef](#)]
9. Zhang, L.S.; Wang, H.L.; Chen, Z.G.; Wong, P.K.; Liu, J.S. Bi_2WO_6 micro/nano-structures: Synthesis, modifications and visible-light-driven photocatalytic applications. *Appl. Catal. B Environ.* **2011**, *106*, 1–13. [[CrossRef](#)]
10. Ma, D.K.; Huang, S.M.; Chen, W.X.; Hu, S.W.; Shi, F.F.; Fan, K. Self-assembled three-dimensional hierarchical umbilicate Bi_2WO_6 microspheres from nanoplates: Controlled synthesis, photocatalytic activities, and wettability. *J. Phys. Chem. C* **2009**, *113*, 4369–4374. [[CrossRef](#)]
11. Nguyen, C.C.; Vu, N.N.; Do, T.-O. Recent advances in the development of sunlight-driven hollow structure photocatalysts and their applications. *J. Mater. Chem. A* **2015**, *3*, 18345–18359. [[CrossRef](#)]
12. Dai, X.J.; Luo, Y.S.; Zhang, W.D.; Fu, S.Y. Facile hydrothermal synthesis and photocatalytic activity of bismuth tungstate hierarchical hollow spheres with an ultrahigh surface area. *Dalton Trans.* **2010**, *39*, 3426–3432. [[CrossRef](#)] [[PubMed](#)]
13. Li, X.N.; Huang, R.K.; Hu, Y.H.; Chen, Y.J.; Liu, W.J.; Yuan, R.S.; Li, Z.H. A templated method to Bi_2WO_6 hollow microspheres and their conversion to double-shell $\text{B}_2\text{O}_3/\text{Bi}_2\text{WO}_6$ hollow microspheres with improved photocatalytic performance. *Inorg. Chem.* **2012**, *51*, 6245–6250. [[CrossRef](#)] [[PubMed](#)]
14. Shang, M.; Wang, W.Z.; Xu, H.L. New Bi_2WO_6 nanocages with high visible-light-driven photocatalytic activities prepared in refluxing EG. *Cryst. Growth Des.* **2009**, *9*, 991–996. [[CrossRef](#)]
15. Wu, J.; Duan, F.; Zheng, Y.; Xie, Y. Synthesis of Bi_2WO_6 nanoplate-built hierarchical nest-like structures with visible-light-induced photocatalytic activity. *J. Phys. Chem. C* **2007**, *111*, 12866–12971. [[CrossRef](#)]

16. Wang, D.J.; Guo, L.; Zhen, Y.Z.; Yue, L.L.; Xue, G.L.; Fu, F. AgBr quantum dots decorated mesoporous Bi₂WO₆ architectures with enhanced photocatalytic activities for methylene blue. *J. Mater. Chem. A* **2014**, *2*, 11716–11727. [[CrossRef](#)]
17. Kudo, A.; Tsuji, I.; Kato, H. AgInZn₇S₉ solid solution photocatalyst for H₂ evolution from aqueous solutions under visible light irradiation. *Chem. Commun.* **2002**, *17*, 1958–1959. [[CrossRef](#)]
18. Fu, H.B.; Yao, W.Q.; Zhang, L.W.; Zhu, Y.F. The enhanced photoactivity of nanosized Bi₂WO₆ catalyst for the degradation of 4-chlorophenol. *Mater. Res. Bull.* **2008**, *43*, 2617–2625. [[CrossRef](#)]
19. Tang, J.W.; Zou, Z.G.; Ye, J.H. Photocatalytic decomposition of organic contaminants by Bi₂WO₆ under visible light irradiation. *Catal. Lett.* **2004**, *92*, 53–56. [[CrossRef](#)]
20. Liu, S.J.; Hou, Y.F.; Zheng, S.L.; Zhang, Y.; Wang, Y. One-dimensional hierarchical Bi₂WO₆ hollow tubes with porous walls: Synthesis and photocatalytic property. *Cryst. Eng. Comm.* **2013**, *15*, 4124–4130. [[CrossRef](#)]
21. Dong, F.; Zheng, A.M.; Sun, Y.J.; Fu, M.; Jiang, B.Q.; Ho, W.K.; Lee, S.C.; Wu, Z.B. One-pot template-free synthesis, growth mechanism and enhanced photocatalytic activity of monodisperse (BiO)₂CO₃ hierarchical hollow microspheres self-assembled with single-crystalline nanosheets. *Cryst. Eng. Comm.* **2012**, *14*, 3534–3544. [[CrossRef](#)]
22. Li, H.X.; Bian, Z.F.; Zhu, J.; Zhang, D.Q.; Li, G.S.; Huo, Y.N.; Li, H.; Lu, Y.F. Mesoporous titania spheres with tunable chamber structure and enhanced photocatalytic activity. *J. Am. Chem. Soc.* **2007**, *129*, 8406–8407. [[CrossRef](#)] [[PubMed](#)]
23. Yang, H.G.; Zeng, H.C. Preparation of hollow anatase TiO₂ nanospheres via Ostwald Ripening. *J. Phys. Chem. B* **2004**, *108*, 3492–3495. [[CrossRef](#)]
24. Hu, J.; Chen, M.; Fang, X.S.; Wu, L.M. Fabrication and application of inorganic hollow spheres. *Chem. Soc. Rev.* **2011**, *40*, 5472–5491. [[CrossRef](#)] [[PubMed](#)]
25. Tian, G.H.; Chen, Y.J.; Zhou, W.; Pan, K.; Dong, Y.Z.; Tian, C.G.; Fu, H.G. Facile solvothermal synthesis of hierarchical flower-like Bi₂MoO₆ hollow spheres as high performance visible-light driven photocatalysts. *J. Mater. Chem.* **2011**, *21*, 887–892. [[CrossRef](#)]
26. Xu, Y.M.; Zhang, Y.W.; Zhou, Y.M.; Xiang, S.M.; Wang, Q.L.; Zhang, C.; Sheng, X.L. CeO₂ hollow nanospheres synthesized by a one pot template-free hydrothermal method and their application as catalyst support. *RSC Adv.* **2015**, *5*, 58237–58245. [[CrossRef](#)]
27. Zhou, X.; Li, X.W.; Sun, H.B.; Sun, P.; Liang, X.S.; Liu, F.M.; Hu, X.L.; Lu, G.Y. Nanosheet-assembled ZnFe₂O₄ hollow microspheres for high-sensitive acetone sensor. *ACS Appl. Mater. Interfaces* **2015**, *7*, 15414–15421. [[CrossRef](#)] [[PubMed](#)]
28. Ma, Z.C.; Wang, L.M.; Chu, D.Q.; Sun, H.M.; Wang, A.X. Template-free synthesis of complicated double-wall Cu₂O hollow spheres with enhanced visible photocatalytic activities. *RSC Adv.* **2015**, *5*, 8223–8227. [[CrossRef](#)]
29. Zheng, Z.K.; Huang, B.B.; Qin, X.Y.; Zhang, X.Y.; Dai, Y. Facile synthesis of SrTiO₃ hollow microspheres built as assembly of nanocubes and their associated photocatalytic activity. *J. Colloid Interface Sci.* **2011**, *358*, 68–72. [[CrossRef](#)] [[PubMed](#)]
30. Liu, J.; Zhang, G.K.; Yu, J.C.; Guo, Y.D. In situ synthesis of Zn₂GeO₄ hollow spheres and their enhanced photocatalytic activity for the degradation of antibiotic metronidazole. *Dalton Trans.* **2013**, *42*, 5092–5099. [[CrossRef](#)] [[PubMed](#)]
31. Dai, K.; Lu, L.H.; Dong, J.; Ji, Z.Y.; Zhu, G.P.; Liu, Q.Z.; Liu, Z.L.; Zhang, Y.X.; Li, D.P.; Liang, C.H. Facile synthesis of a surface plasmon resonance enhanced Ag/AgBr heterostructure and its photocatalytic performance with 450 nm LED illumination. *Dalton Trans.* **2013**, *42*, 4657–4662. [[CrossRef](#)] [[PubMed](#)]
32. Zhang, G.Y.; Feng, Y.; Wu, Q.S.; Xu, Y.Y.; Gao, D.Z. Facile fabrication of flower-shaped Bi₂WO₆ superstructures and visible-light-driven photocatalytic performance. *Mater. Res. Bull.* **2012**, *47*, 1919–1924. [[CrossRef](#)]
33. Merka, O.; Yarovy, V.; Bahnemann, D.W.; Wark, M. pH-control of the photocatalytic degradation mechanism of Rhodamine B over Pb₃Nb₄O₁₃. *J. Phys. Chem. C* **2011**, *115*, 8014–8023. [[CrossRef](#)]
34. Fu, H.B.; Pan, C.S.; Yao, W.Q.; Zhu, Y.F. Visible-light-induced degradation of Rhodamine B by nanosized Bi₂WO₆. *J. Phys. Chem. B* **2005**, *109*, 22432–22439. [[CrossRef](#)] [[PubMed](#)]

